Available online at www.sciencedirect.com
SCIENCE DIRECT®
Journal of Solid State Chemistry 178 (2005) 2987–2997
JOURNAL OF SOLID STATE CHEMISTRY
www.elsevier.com/locate/jssc

LiB_3O_5 crystal structure at 20, 227 and 377 °C

Yu.F. Shepelev[a], R.S. Bubnova[a], S.K. Filatov[b,*], N.A. Sennova[b], N.A. Pilneva[c]

[a]*Grebenshchikov Institute of the Silicate Chemistry of the Russian Academy of Sciences, Ul. Odoevskogo 24 (2), St. Petersburg, 199155, Russia*
[b]*Department of Crystallography, St. Petersburg State University, University Emb. 7/9, St. Petersburg, 199034, Russia*
[c]*Institute of Mineralogy and Petrography RAS, Novosibirsk, Russia*

Received 30 March 2005; received in revised form 24 May 2005; accepted 13 June 2005
Available online 15 August 2005

Abstract

Crystal structure of LiB_3O_5 (a framework of $[B_3O_5]^-$ rings and Li atoms located in interspaces) was refined at high temperatures using single-crystal X-ray diffraction, Mo$K\alpha$-radiation, anharmonic approximation, orthorhombic; $Pna2_1$; $Z = 4$; 20 °C ($a = 8.444$, $b = 7.378$, $c = 5.146$ Å, 1411 $F(hkl)$, $R = 0.022$); 227 °C ($a = 8.616$, $b = 7.433$, $c = 5.063$ Å, 1336 $F(hkl)$, $R = 0.026$), 377 °C ($a = 8.746$, $b = 7.480$, $c = 5.013$ Å, 1193 $F(hkl)$, $R = 0.035$). A high mobility of Li atoms and their highly asymmetric vibrations are revealed. Ellipsoid of Li thermal vibrations is oviform. Li is shifted on heating to 0.26 Å mainly along a-axis causing high thermal expansion in this direction; Li temperature factors are multiplied by 4 on heating. Rigid boron–oxygen groups in LiB_3O_5 remain practically stable on heating similar to α-$Na_2B_8O_{13}$ and α-CsB_5O_8. At the same time these groups rotate relative to each other like hinges leading to extremely anisotropic thermal expansion ($\alpha_a = 101$, $\alpha_b = 31$, $\alpha_c = -71$, $\alpha_v = 60 \times 10^{-6}$ °C^{-1}, 20–530 °C, HTXRPD data).

Keywords: LiB_3O_5; Borates; Crystal structure; Single-crystal X-ray diffraction; Thermal behavior; Anharmonic atomic vibrations; Nonlinear optics; HTXRPD

1. Introduction

An interest in the study of nonlinear optical effects, in particular, to the problem of generation of the second harmonic (SHG) of laser radiation, has grown considerably nowadays, especially as solid-state laser sources started replacing gas and ion laser sources for various applications and they need frequency conversion devices.

Lithium triborate exhibits excellent nonlinear optical properties [1–3], luminescent properties [4,5], spontaneous polarization and moderate piezoelectric coefficients [6,7] parallel with high laser damage threshold [8] required for many applications. Crystals of LiB_3O_5 are widely used as nonlinear optical units and materials for integrated optical wave guides in laser weapon, welder, radar, surgery, communication, etc. So, there are lot various studies of LiB_3O_5, for example, the study of synthesis and crystal growth of LiB_3O_5 [9–12], infrared spectra [13,14], dielectric properties [15], specific heat at low temperatures [16], structure and chemistry of LiB_3O_5 optical surfaces [17], etc. According to [1], LiB_3O_5 may operate better than potassium dihydrogen phosphate and β-barium metaborate crystals for frequency conversions of various laser radiation.

The crystal structure of LiB_3O_5 was studied at room temperature [18,19–22], paying special attention [20–22] to the distribution of electron density. The structure consists of a framework of $[B_3O_5]^-$ three-fold (triborate) rings [23] consisting of two triangles and a tetrahedron, and Li atoms located in the interspaces of this framework. All triborates of univalent metals except for the two modifications of sodium triborate [24,25] are also built up from such rings. These are the topologically identical three-dimensional frameworks of LiB_3O_5 [18],

*Corresponding author.
E-mail address: filatov@crystal.pu.ru (S.K. Filatov).

0022-4596/$ - see front matter © 2005 Published by Elsevier Inc.
doi:10.1016/j.jssc.2005.06.017

CsB_3O_5 [26,27], $CsLiB_6O_{10}$ [28], TlB_3O_5 [29], α-, β-RbB_3O_5 [30,31], and also another framework of KB_3O_5 [32]. The first four compounds exhibit excellent nonlinear optical properties. It seems that α- and β-RbB_3O_5 are potential nonlinear optical materials. The correlation of CsB_3O_5, $CsLiB_6O_{10}$, and LiB_3O_5 crystal structures and their nonlinear optical properties was studied [14,33,34]. It is noted [33] that as the structures contain the same B–O rings, the difference in nonlinear optical properties arises from a contribution of different cations. According to [34], the contribution of cations to the second-harmonic generation becomes slightly more pronounced with the increase of their radius.

The application of new promising materials at elevated temperatures and their crystal growth require the knowledge of their crystal structure in correlation with physical properties and information relating to their thermal expansion. High-temperature X-ray powder diffraction [35,36], dilatometric studies [36], and differential thermal analysis [36] of LiB_3O_5 were provided. The first studies of thermal behavior of borate crystal structures were performed by us for α-$Na_2B_8O_{13}$ [37] comprising triborate and pentaborate groups and α-CsB_5O_8 [38] comprising pentaborate groups. These studies allowed us to state thermal stability of the rigid boron–oxygen groups on heating [39]. According to [10], the percentage of various B–O groups in the LiB_3O_5 melt also depends upon thermal treatment: when the melt is heated a few degrees above the melting point it essentially contains $(B_3O_5)^{-1}$ groups, on heating up to 900 °C these groups get transformed to the ones corresponding to $Li_2B_4O_7$ and $Li_3B_7O_{12}$.

Nonlinear optical effects might be caused by the anharmonicity of atomic thermal displacements that can be seen in thermal expansion tensor and in deviations from Gaussian shape of the probability density function of atomic thermal displacement factors. In the present work the single crystal and powder X-ray diffraction studies at high temperatures of LiB_3O_5 are given. This is the first study of borate crystal structure at high temperatures in anharmonic approximation.

2. Experimental

The crystals of LiB_3O_5 were grown on a seed from the solution-melt using the method of temperature lowering. Polymolybdates were used as a solvent. The seed was oriented along [001] axis. Li_2CO_3 (99.97%), B_2O_3 (99.997%) and MoO_3 (99.995%) were used as precursors. The cooling rate varied in the range of 0.5–1 °C/24 h. The temperature variations were ±0.05 °C. Crystal growth was carried out in a three-zone furnace and lasted for 30–35 days. The obtained colorless crystals had well-developed forms and weighed more than 200 g.

Experimental intensity data were collected at 20, 227 and 377 °C on the automatic single-crystal diffractometer with the perpendicular beam scheme using graphite-monochromatized Mo$K\alpha$-radiation ($\lambda = 0.71069$ Å). The crystal (see Table 1) placed on a glass capillary by a special high-temperature glue was blown by hot air while being measured. Temperature was checked by a thermocouple located on a tube output giving hot air to the crystal. The absolute accuracy of temperature was about 10 °C, the relative temperature variations were 4 °C.

Table 1
Experiment details and crystal data

Parameter	20 °C	227 °C	377 °C
Crystal dimensions		$0.7 \times 0.3 \times 0.2\,mm^3$	
Formula weight		119.37	
Symmetry, Z		$Pna2_1$, $Z = 4$	
a (Å)	8.444(5)	8.616(5)	8.746(7)
b (Å)	7.378(4)	7.433(5)	7.480(6)
c (Å)	5.146(3)	5.063(3)	5.013(5)
Refinement in anharmonic approximation			
General number of F (hkl) with $F>3\sigma(F)$	1411	1336	1193
R-factor (%)	2.19	2.56	3.01
R_w-factor (%)	2.57	3.16	3.52
General number of F (hkl) with $F>3\sigma(F)$ Accepted by LSQ	1310	1220	1106
R-factor (%)	1.68	2.04	2.48
R_w-factor (%)	1.71	2.08	2.47
Sig 1-factor	0.82	0.96	1.05
Refinement in anisotropic approximation			
General number of F (hkl) with $F>3\sigma(F)$	1411	1336	1193
R-factor (%)	2.42	2.88	3.33
R_w-factor (%)	2.86	3.71	3.99
General number of F (hkl) with $F>3\sigma(F)$ Accepted by LSQ	1306	1228	1098
R-factor (%)	2.01	2.37	2.83
R_w-factor (%)	2.15	2.60	2.87
Sig 1-factor	0.95	1.16	1.24
Refinement in isotropic approximation			
General number of F (hkl) with $F>3\sigma(F)$	1411	1336	1193
R-factor (%)	4.72	8.66	10.86
R_w-factor (%)	5.83	13.11	16.01
General number of F (hkl) with $F>3\sigma(F)$ Accepted by LSQ	1243	1175	1052
R-factor (%)	6.04	7.16	9.19
R_w-factor (%)	8.62	9.60	12.21
Sig 1-factor	2.58	3.99	4.76

The stability of a primary beam intensity was checked up by a regular control of reflection intensity measurements and the subsequent correction on drifting was performed. The integrated intensity I_0 was separated from the measured reflex profile (15 points), I_x, by a method of profile specification [40]. No absorption correction ($\mu = 0.23\,\mathrm{mm}^{-1}$) was performed. 1411–1193 reflections with $F \geqslant 3(\sigma(F))$ were used in the structure determination. Atomic coordinates from Ref. [18] were used as the initial ones. In the present polar space group the origin of coordinates is fixed on z-axis by the following condition:

$$\sum_{i=1}^{\mathrm{NA}} z_i = \mathrm{const},$$

where NA is the number of atoms. The positional and anisotropic thermal parameters of all atoms were refined by a full-matrix block-diagonal least-squares procedure using the modified version of the ORFLS program [41]. For the other structural calculations the AREN-90 program package [42] was used. The structure was refined in anharmonic approximation using Edgeworth model [43]. The R-factor was reduced to 1.68% at 20 °C calculated using 1310 unique reflections in comparison with $R = 9.7\%$ from the first study [18] and 1.88% for 1130 reflections (2.04% for 1229 reflections) from [20,21]. Experimental details, crystal data and the R-factors for refinements in isotropic, anisotropic and anharmonic approximations of LiB_3O_5 are given in Table 1. The refined atomic coordinates and equivalent thermal parameters at different temperatures are listed in Table 2. Atomic root-mean-square displacements (Å) are given in Table 3. Further details of the crystal structure investigations can be obtained from the Fachinformationszentrum Karlsruhe, 76344 Eggenstein-Leopoldshafen, Germany, (fax: (49) 7247-808-666; e-mail: crysdata@fiz.karlsruhe.de) on quoting the depository numbers CSD 415199, 415200, 415201.

Heat treatments of LiB_3O_5 powder samples were performed in the electric furnace in a platinum crucible at 520 and 580 °C.

Thermal expansion of the LiB_3O_5 was studied in situ by high-temperature X-ray powder diffraction (HTXRPD) using DRON-3 diffractometer equipped with a high-temperature KRV-1100 chamber, Cu$K\alpha$-radiation. The sample was prepared from a heptan suspension on Pt plate. Intensity measurements were performed in air in the range 20–770 °C with the 65 K/h average heating rate, the study being more detailed (step 40 °C) in contrast to the previous studies [35,36] (100 °C). Temperature dependences for unit-cell parameters in the temperature range 20–710 °C are given in Fig. 1. Sections of the polar figure of the coefficients of thermal expansion by the *ab* and *ac* planes are given in Figs. 3 and 4.

Table 2
Atomic parameters of the LiB_3O_5 crystal structure at 20, 227 and 377 °C. $B_{eq} = \left(\Sigma\sqrt{\left(\overline{U_i^2}\right)}\right)/3$

Atom	x/a	y/b	z/c	B_{eq} (Å^2)
20 °C				
Li1	.4120(2)	.5669(2)	.0000(0)	1.63(2)
B1	.50983(6)	.83545(6)	.3525(3)	.547(6)
B2	.69434(5)	.05688(5)	.5489(3)	.444(5)
B3	.65725(5)	.75137(6)	.7321(3)	.485(5)
O1	.58671(4)	.99559(4)	.3450(3)	.681(4)
O2	.38351(4)	.79517(4)	.1966(3)	.613(4)
O3	.55827(4)	.70208(4)	.5279(3)	.648(4)
O4	.73880(4)	.90976(4)	.7332(3)	.526(4)
O5	.66116(4)	.62494(4)	.9268(3)	.614(4)
227 °C				
Li1	.3998(4)	.5645(3)	.01285(0)	3.98(5)
B1	.51021(7)	.83541(7)	.3522(7)	.925(8)
B2	.69169(6)	1.05537(7)	.5485(7)	.752(7)
B3	.65714(6)	.75120(7)	.7339(7)	.790(7)
O1	.58783(6)	.99258(5)	.3407(7)	1.202(6)
O2	.38549(6)	.79730(5)	.1964(7)	1.074(6)
O3	.55743(6)	.70286(5)	.5295(7)	1.166(6)
O4	.73472(5)	.90985(5)	.7367(7)	.914(5)
O5	.66680(5)	.62222(5)	.9251(7)	1.092(6)
377 °C				
Li1	.3870(6)	.5627(4)	.02755(0)	6.4(1)
B1	.51026(9)	.83512(9)	.353(1)	1.21(1)
B2	.68917(8)	1.05489(9)	.548(1)	.995(9)
B3	.65730(7)	.75098(9)	.735(1)	1.0(1)
O1	.58768(7)	.99078(7)	.339(1)	1.568(8)
O2	.38682(7)	.79821(6)	.196(1)	1.478(8)
O3	.55699(7)	.70327(7)	.532(1)	1.587(9)
O4	.73164(6)	.91016(6)	.738(1)	1.226(7)
O5	.67118(6)	.62094(7)	.924(1)	1.476(8)

Table 3
Atomic root-mean-square displacements (Å) in the LiB_3O_5

Atom	20 °C	227 °C	377 °C	Atom	20 °C	227 °C	377 °C
Li1	.097	.129	.142	O1	.074	.094	.111
	.129	.175	.203		.075	.103	.118
	.188	.322	.428		.121	.161	.181
B1	.073	.093	.105	O2	.071	.093	.108
	.079	.102	.117		.075	.098	.112
	.094	.126	.145		.111	.149	.177
B2	.062	.081	.094	O3	.069	.092	.106
	.073	.098	.108		.074	.099	.111
	.086	.110	.130		.119	.161	.190
B3	.065	.084	.098	O4	.060	.079	.095
	.074	.094	.103		.076	.101	.116
	.092	.118	.140		.102	.134	.154
				O5	.061	.079	.092
					.076	.100	.112
					.117	.158	.186

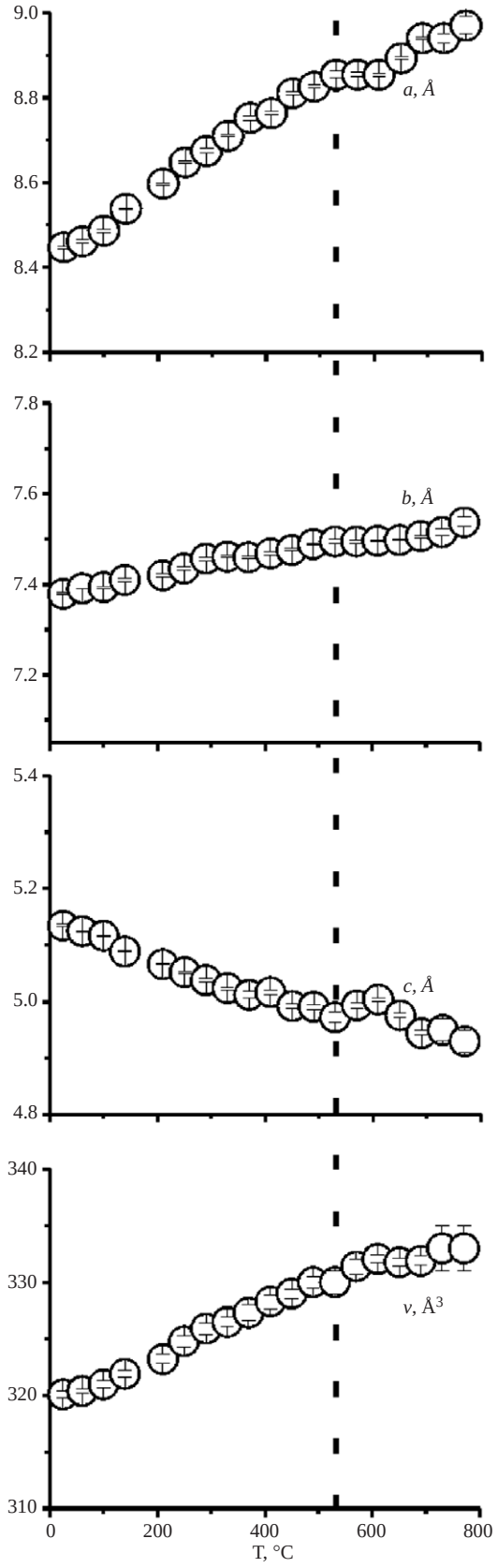

Fig. 1. Temperature dependence of the unit-cell parameters of LiB_3O_5.

3. HTXRPD studies

Selective diffraction patterns of HTXRPD study of LiB_3O_5 are presented in Fig. 2. The intensities of certain reflections of LiB_3O_5 changed significantly on heating, for instance, line (1 1 1) (Fig. 2).

At 650 ± 20 °C the first slight traces of $Li_3B_7O_{12}$ arise, they are denoted by circles (Fig. 2). On further heating more peaks of $Li_3B_7O_{12}$ appear. Thus LiB_3O_5 starts to decompose. This fact disagrees with the data of Lin Wei et al. [35], wherein LiB_3O_5 decomposes above 500 °C forming $Li_2B_4O_7$. For this reason the decomposition of LiB_3O_5 was investigated by an annealing and quenching method. After isothermal heat treatments of LiB_3O_5 powder samples at 520 °C for 130 h and 580 °C for 95 h, traces of $Li_2B_4O_7$ were observed and no traces of $Li_3B_7O_{12}$ have been found.

The obtained discrepancy could be caused by various temperature conditions. According to the phase diagram of Li_2O–B_2O_3 system [44], the LiB_3O_5 and $Li_4B_{10}O_{17}$ compounds are formed by a solid-state reaction $LiB_3O_5 \leftrightarrow Li_2B_4O_7 + Li_2B_8O_{13}$ and $Li_4B_{10}O_{17} \leftrightarrow Li_2B_4O_7 + LiB_3O_5$ at 595 ± 20 °C and 696 ± 4 °C, respectively. It should be noted that a structure of the compound reported to have the Li_2O:B_2O_3 ratio of 2:5 ($Li_4B_{10}O_{17}$) in the Li_2O–B_2O_3 system [44,45] showed it has the 3:7 ratio and the $Li_3B_7O_{12}$ formula [46] and we apply the last corrected formula here. Hence, LiB_3O_5 being metastable below about 600 °C starts to decay forming $Li_2B_4O_7$ or $Li_3B_7O_{12}$ depending on heating rate. It is notable when investigating LiB_3O_5 by the annealing and quenching method we observe formation of

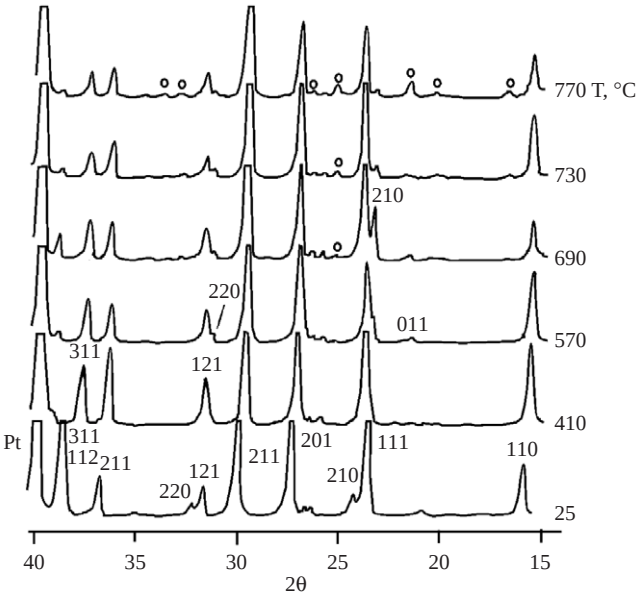

Fig. 2. High-temperature X-ray diffraction patterns for LiB_3O_5. $Li_3B_7O_{12}$ peaks are indicated by circles.

$Li_2B_4O_7$ that is stable at these temperatures in accord with the phase diagram [44]. The data on solid-state phase equilibria of the LiB_3O_5 and $Li_3B_7O_{12}$ compounds are insufficient in other versions of phase diagram of the Li_2O–B_2O_3 system [45,47], at that, the low-temperature region is not considered in [45].

The temperature dependencies for the a and c unit-cell parameters and V cell volume are practically linear, although the small bends starting from $530 \pm 20\,^{\circ}C$ are visible (Fig. 1). This temperature is close to a glass-transition temperature of LiB_3O_5 melt (470 °C [48]). Such bends (special points) have already been found by us for borates of K, Rb [49] and Na. It is believed that the nature of the special or singular points lies in a drastic increase in the ionic mobility in the crystals, that leads to the onset of the metastable phase transition, just as it occurs with a glass at the glass-transition temperature.

Thermal expansion coefficients calculated with the linear approximation of temperature dependencies of the unit-cell parameters in the temperature range of 20–530 °C are the following: $\alpha_a = 101$, $\alpha_b = 31$ $\alpha_c = -71 \times 10^{-6}\,^{\circ}C^{-1}$. Thus, thermal expansion of LiB_3O_5 has extremely anisotropic character; the structure maximally expands along a-axis and contracts along c-axis. The volume thermal expansion is $\alpha_v = 60 \times 10^{-6}\,^{\circ}C^{-1}$. The revealed character of anisotropy of thermal expansion is similar to [35,36] (Table 4), although α_v of [36] is nearly two times smaller than in the present study and in [35]. $\langle\alpha\rangle = \alpha_V/3 = 20 \times 10^{-6}\,^{\circ}C^{-1}$ is practically twice larger than $\alpha = 12 \times 10^{-6}\,^{\circ}C^{-1}$ obtained by dilatometry in [36]. It should be noticed that the publications [35,36] are less detailed (temperature step 100 °C). Furthermore this difference can be understood by the high porosity of the bar which results in a decreasing of the measured expansion coefficient.

4. Thermal changes in the crystal structure

To examine a structure relaxation of LiB_3O_5 (Figs. 3, 4) with respect to the temperature increasing, we have taken into consideration the thermal changes of bond distances and angles and anharmonic displacement parameters for all atoms with emphasis on thermal structural behavior of triborate groups. There might be two mechanisms for an extraordinary intensive contraction along c-axis as it was pointed out in [35]. These are the changing of B–O–B angles and the rotation of the planes of triborate rings towards the ab plane. One of the aims of this work is to find which mechanism plays the principal role.

Table 4
Comparison of thermal expansion coefficients

Coefficients ($\times 10^{-6}\,^{\circ}C^{-1}$)	Present study 20–530 °C step 40 °C	Mathews et al. [36] 20–612 °C step 100 °C	Lin Wei et al. [35] 17–790 °C* step 100 °C
α_a	101	65.77	108.2
α_b	31	29.08	33.6
α_c	−71	−62.51	−88.0
α_v	60	32.32	54
$\langle\alpha\rangle$	20	11 ($\alpha = 12 \times 10^{-6}\,^{\circ}C^{-1}$ dilatometry)	18

*Coefficients are given for 50 °C.

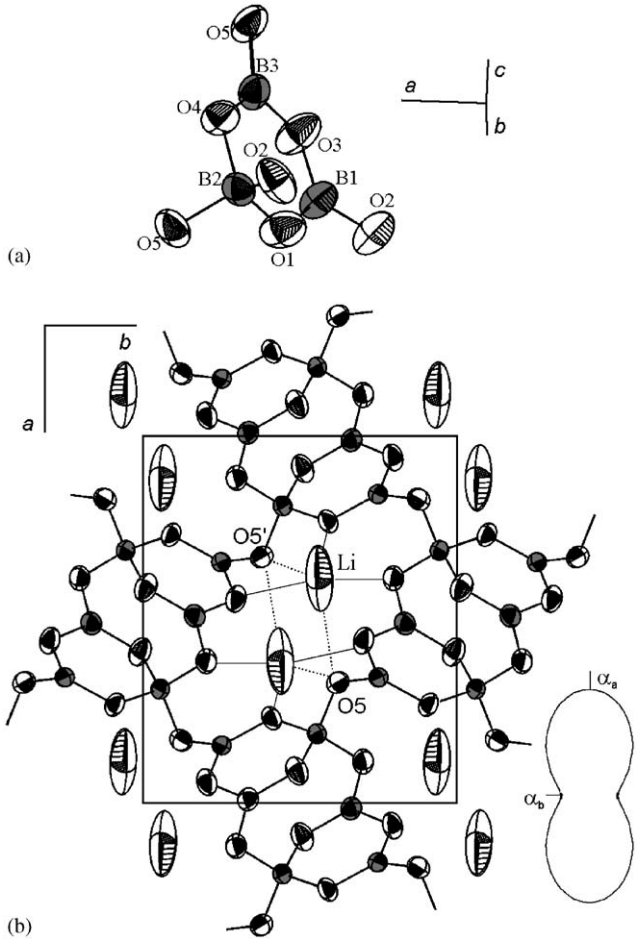

Fig. 3. Triborate group (a) and projection of the LiB_3O_5 crystal structure onto ab plane (b) at 377 °C. Boron atoms are light gray. Ellipsoids are given with 80% probability.

4.1. Thermal behavior of Li atoms

There is a symmetrically non-equivalent Li atom in the structure [20,21]. Li coordination at the room temperature is considered in [20,21] as a distorted tetrahedron where Li atom is displaced from the tetrahedron center towards O2O3O4 plane (Table 5, Fig. 3). Thus, Li atoms at 20 °C are coordinated by four oxygen atoms with Li–O bond length being 1.979–2.180 Å (Table 5), the next oxygen O5′ atom being 2.684 Å away from Li. LiO_5 polyhedra linked by O5 atoms form chains within the

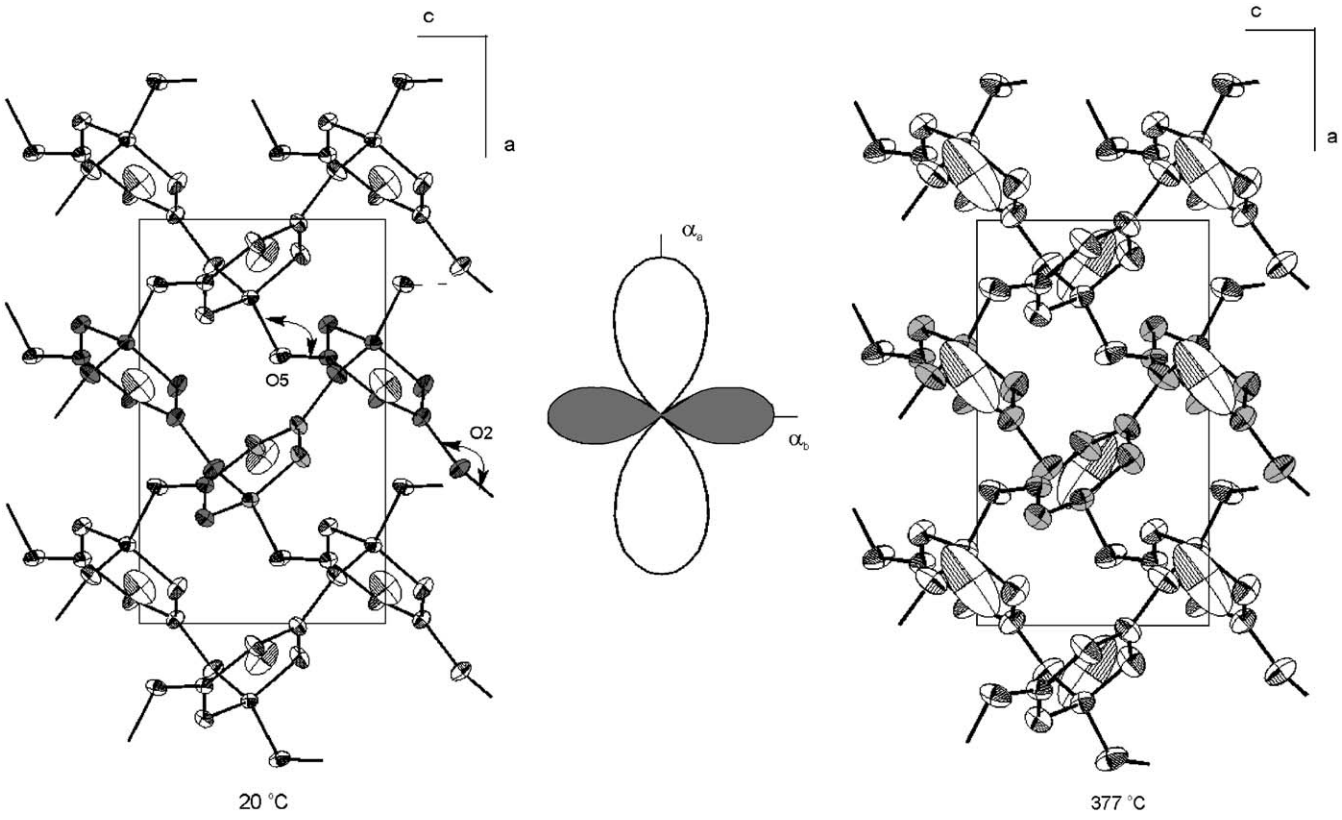

Fig. 4. LiB_3O_5 structure projection onto *ac* plane at 20 and 377 °C. Ellipsoids are given with 80% probability.

channels, alternating with the chains of triborate group (Fig. 5). At 227 °C Li moves 0.25 Å towards the O2O3O4 plane, and its coordination becomes triangular (d(Li–O) = 1.968–2.003 Å). The fourth O5 oxygen constituting tetrahedron at 20 °C moves to 2.381 Å away from Li (Table 5, Fig. 6(a)) and the fifth O5′ oxygen is 2.6 Å away from Li (Fig. 3). At 377 °C Li is coordinated by three oxygens, forming the plane LiO_3 triangle in the first coordination sphere, and by two oxygens on both sides of this triangle (second coordination sphere). The changing of Li–O bond lengths on heating is shown in Fig. 6(a). It is seen that three shortest bonds practically donot change on heating while the longer Li–O5 bond increases much more leading to the changing of Li coordination from 4 to 3 on heating.

Lithium atoms are rarely coordinated by three oxygens at room conditions. For example, the three-fold coordination of lithium atom by oxygens with $\langle d(\text{Li–O})\rangle = 1.888$ Å occurs in $LiBaB_9O_{15}$ [50]. It is noted that Li coordination also becomes triangular in a $LiAlSi_2O_6 \cdot H_2O$ bikitaite above 480 °C as it was noticed by Ferro in accordance with Ref. [50]. The Li coordination number tends to become triangular in $Li_2B_4O_7$ on heating up to 500 °C [51]. Decreasing of cationic coordination number is usual on heating. It was noted for diopside and hedenbergite [51], two bond distances of eight-fold polyhedron in diopside and hedenbergite increase with a much higher rate than the other bond lengths at high temperatures, so that the coordination becomes nearer to six-fold, rather than eight-fold [52]. Similarly, the tendency toward the coordination number decreasing was also manifested in NaO_8 polyhedra of $Na_2B_8O_{13}$ [37] and CsO_9 in CsB_5O_8 [38].

In LiO_4 polyhedra the average Li–O bond length changes from 2.044 to 2.118 on heating up to 377 °C. In LiO_5 polyhedra the values are 2.172 and 2.209 Å, correspondingly, that is comparable to the changing of the average Na–O bond length on heating in the structure of α-$Na_2B_8O_{13}$ [37]. Bond-valence sums for Li atoms (Table 5) in the structure of LiB_3O_5 were calculated using the bond-valence parameters for B–O and Li–O bonds from [53]. For the four shortest Li–O bonds the value amounts 0.856 v.u. For LiO_5 polyhedra the bond-valence sum of Li is 0.893 v.u. The bond-valence sums at elevated temperatures are 0.714 and 0.712 v.u. at 227 and 377 °C (three-fold coordination) and 0.849, 0.828 v.u. at 227 and 377 °C (five-fold coordination), respectively. But we have to keep in mind that these values are rough at elevated temperatures because this model was calculated at normal conditions.

Analysis of atomic motions has revealed that coordinates of Li atoms change considerably on heating in comparison with the other atomic coordinates of

Table 5
Bond lengths (Å) in the LiB_3O_5 crystal structure

	20 °C	227 °C	377 °C	Δ*
BO_3 triangles				
B1–$^{\triangle}$O 1	1.3486 (5)	1.3473 (7)	1.349 (1)	0.0004
B1–$^{\triangle}$O 2	1.367 (1)	1.362 (2)	1.363 (4)	−0.004
B1–$^{\triangle}$O$^{\triangle}$3	1.396 (1)	1.393 (3)	1.394 (4)	−0.002
⟨B1–O⟩	1.371	1.367	1.369	−0.002
B3–$^{\triangle}$O 4	1.3564 (5)	1.3556 (6)	1.357 (1)	0.0006
B3–$^{\triangle}$O 5	1.369 (1)	1.364 (3)	1.363 (5)	−0.006
B3–$^{\triangle}$O$^{\triangle}$3	1.391 (1)	1.392 (3)	1.389 (5)	−0.002
⟨B3–O⟩	1.372	1.371	1.370	−0.002
BO_4 tetrahedron				
B2–O$^{\triangle}$1	1.460 (1)	1.457 (3)	1.455 (5)	−0.005
B2–O$^{\triangle}$5	1.461 (1)	1.457 (2)	1.457 (3)	−0.004
B2–O$^{\triangle}$2	1.483 (1)	1.484 (2)	1.483 (3)	0
B2–O$^{\triangle}$4	1.489 (1)	1.488 (3)	1.488 (4)	−0.001
⟨B2–O⟩	1.473	1.472	1.471	−0.003
LiO polyhedron				
Li–O2	1.979 (1)	1.968 (2)	1.953 (3)	−0.026
Li–O3	2.005 (1)	2.022 (2)	2.049 (2)	0.044
Li–O4	2.013 (1)	2.003 (3)	1.999 (5)	−0.014
Li–O5	2.180 (1)	2.381 (3)	2.469 (5)	0.289
⟨Li–O_3⟩	1.999	1.998	2.000	0.001
⟨Li–O_4⟩	2.044	2.094	2.118	0.074
bond valence sums (Li^{IV})**	0.86	≈0.71	≈0.71	
Li–O5′	2.684 (1)	2.571 (3)	2.576 (6)	−0.108
⟨Li–O_5⟩	2.172	2.189	2.209	0.037
bond valence sums (Li^{V})	0.89	≈0.85	≈0.83	

*Δ—the difference between the bond lengths at 377 and 20 °C, accordingly.
**Li^{IV} and Li^{V} – tetrafold and fifthfold coordination of Li atoms.

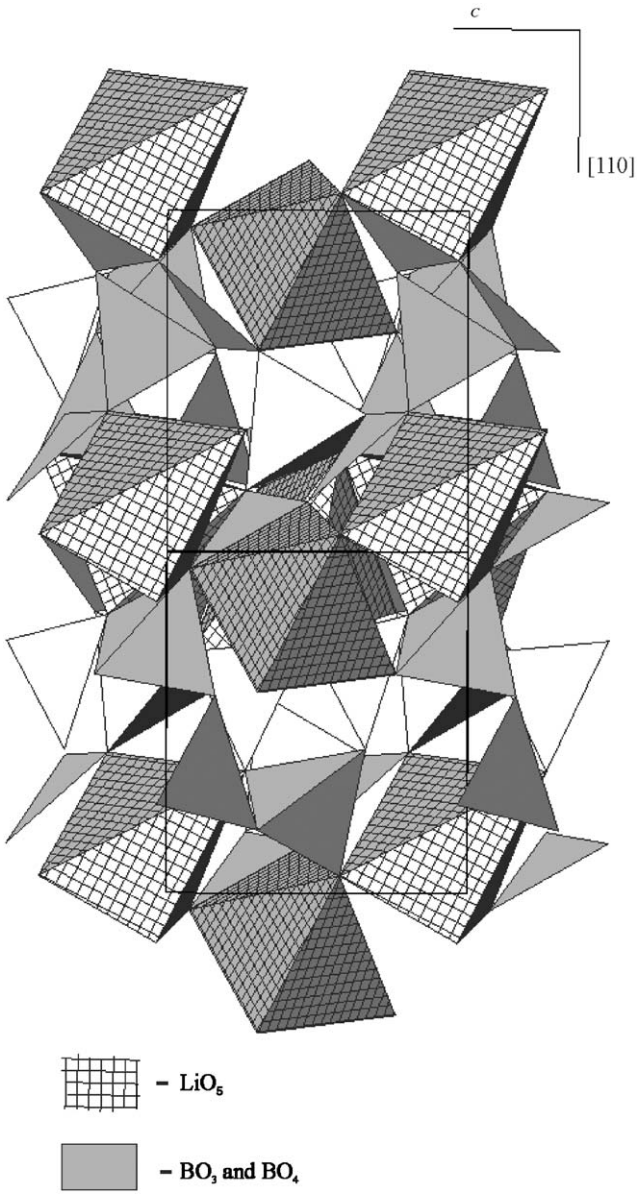

Fig. 5. Chains of LiO_5 polyhedra in LiB_3O_5 crystal structure.

LiB_3O_5 crystal structure. Li atoms shift to approximately 0.26 Å, while the shifts of other atoms in LiB_3O_5 are much smaller, the average one being equal to nearly 0.04 Å. Decreasing intensity reflections on heating mentioned above also could be interpreted as Li motion like oxygen motion in calcite [54].

4.2. Thermal displacement parameters of Li atoms at high temperatures

Li atoms vibrate greatly in comparison with other atoms. Li equivalent displacement factor (B_{eq}) multiplies up more than 4 times on heating to 377 °C (Table 2). It should be noted that the B_{eq} factor increases more sharply than usually. For example the B_{eq} factor for Li is about 1.1 $Å^2$ at room conditions, and this value increases only to about 2.6 $Å^2$ on heating to 400 °C in the $LiAlSi_2O_6$ silicate [52].

Refinement of the structure in anharmonic approximation using Edgeworth model [43] has shown that only anharmonic temperature factors of Li of the third order are statistically significant. Heating mainly affected the coefficient at $h^3(c_{111})$: $-3.7(4)\times10^{-6}$, $-21.8(6)\times10^{-6}$, $-37.1(4)\times10^{-6}$ at 20, 227 and 377 °C, correspondingly. Therefore, the major anharmonicity is at Li atomic displacements along *a*-axis. The anharmonic temperature factors of boron and oxygen atoms of the third order are of the same order as their esd's, as well as the anharmonic temperature factors of the fourth order of all atoms (Li, B, O). The refined figure of Li thermal vibrations is shown in Fig. 6(b,c). It is oviform. Thermal vibrations of Li atoms in $Li_2B_4O_7$ [51] are more harmonic than in LiB_3O_5, which SHG effect is more pronounced. According to "Bond Polarizability theory" ([55] after materials of Dphil. thesis of Jeggo, 1971) the nonlinear behavior of a material is reduced to a sum of contributions from all the chemical bonds within the structure. Thus, highly

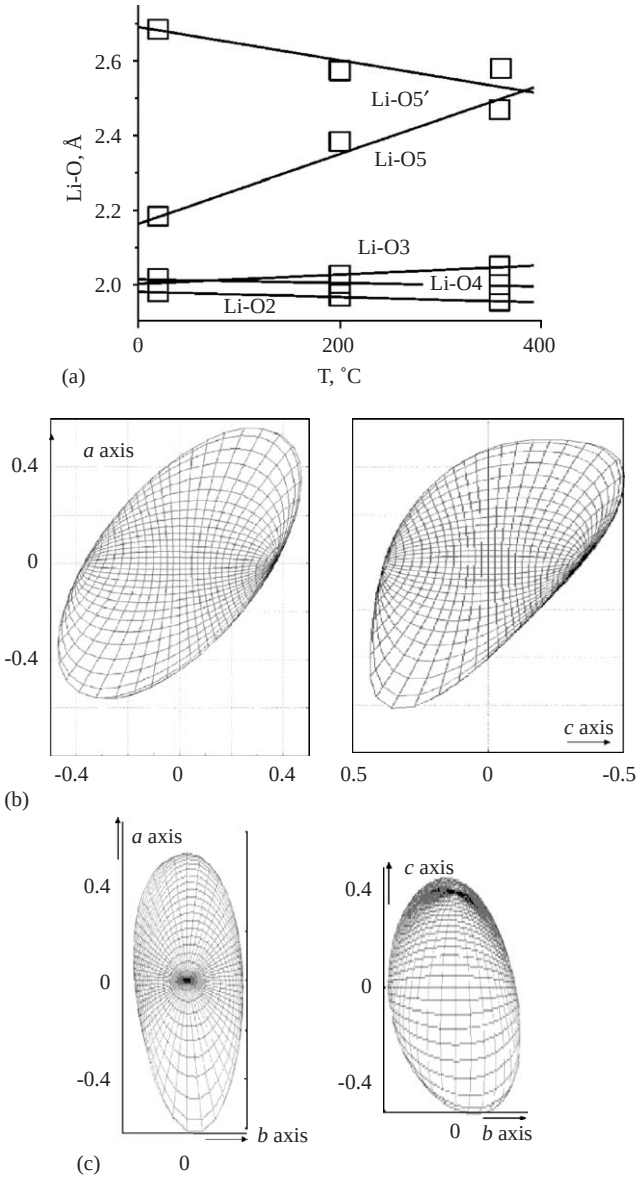

Fig. 6. Li–O bond lengths (a), Li ellipsoid and the figure of thermal vibrations in anharmonic approximation in *ac* plane (b), *ab* and *cb* planes (c) in LiB_3O_5 crystal structure at 377 °C.

asymmetric bonding leads to significantly greater non-linearity. If we assume that the main contribution to the nonlinearity of LiB_3O_5 is provided by Li atoms, then it might be caused by a distorted LiO coordination resulting even in a distorted form of ellipsoid of Li thermal vibration. This might be caused by a high mobility of Li atoms. They are located along *c*-axis in the channels of B–O framework and are dislocated from the center of these channels forming shorter bonds with O2, O3 and O4 and longer bonds with O5 and O5′.

4.3. Thermal changes in B–O framework

There are three symmetrically independent B atoms: the B1 and B3 atoms are coordinated by three O atoms in a triangular arrangement, whereas the B2 atoms are tetrahedrally coordinated by four O atoms. At room conditions the average B–O bond lengths (Fig. 7) equal to 1.37 and 1.473 Å in the triangles and tetrahedron, respectively, and angles (109° in BO_4 tetrahedron and 120° in BO_3 triangles) are typical for borate structures [39,56], although individual bonds are scattered greatly (Tables 5, 6). According to [20,21], O2, O3 and O4 oxygen atoms form weaker bonds with boron in contrast to O5 having strong bonds with boron atoms and, therefore, weaker bonds with lithium atoms. It should be noted that this O5 atom is the bridge between two chains of triborate groups. According to the regularity discussed by Filatov and Bubnova in [39], B–O bond length in a triangle is shortened if the other neighboring atom of the oxygen is boron in tetrahedral coordination (Table 3) which could be caused by the fact that the valence effort in a triangle is stronger than in a tetrahedron. In the structure of the LiB_3O_5 the average B–O bond length in the triangles is 1.360 Å if oxygen

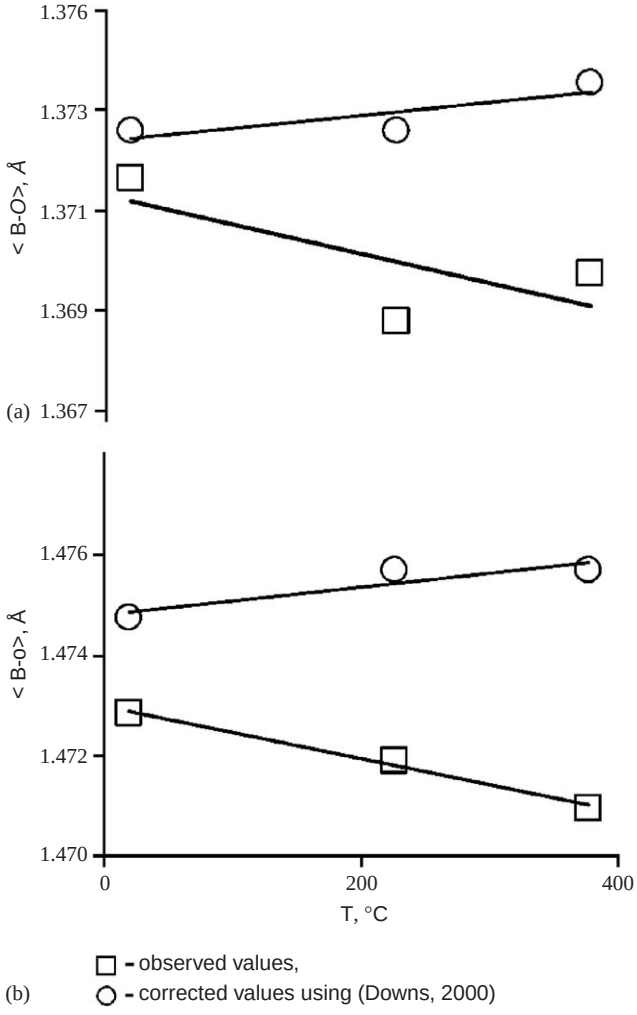

Fig. 7. B–O bond lengths in triangles (a) and tetrahedra (b) in LiB_3O_5 crystal structure.

atoms link tetrahedral and triangular boron polyhedra ($O^{\triangle}$) against 1.394 Å at 20 °C in the case when they link a triangle with a triangle ($^{\triangle}O^{\triangle}$). These values are close to the bonds variation data of [39], i.e. 1.347–1.371 and 1.374–1.387 Å, respectively. When temperature increases, the individual bond lengths show the same systematical variations as at room temperature.

4.3.1. B–O rigid body motion correction to thermal bond lengths contraction

The observed B–O bond lengths computed from the refined positions of the atoms (Table 5) slightly change with temperature. Even a small contraction of the most part of individual and mean bonds is observed like in previously studied α-$Na_2B_8O_{13}$ [37] and α-CsB_5O_8 [38]. This contraction could be attributed to the model of rigid-body motion [57]. Bond lengths were corrected according to the model of rigid-body motion using the formula given in [58,59]

$$R^2_{corr} = R^2_{obs} + 3/8\pi^2(B_{eq}(A) - B_{eq}(C)),$$

where R_{corr} and R_{obs} are corrected and observed B–O bond lengths, correspondingly; $B_{eq}(A)$ and $B_{eq}(C)$ are equivalent temperature factors of anion (oxygen) and cation (boron), correspondingly. After applying this correction, the mean B–O bond lengths tend to increase slightly on heating. Mean B–O bond lengths as a function of temperature are given on Fig. 7 for BO_3 triangles (*a*) and BO_4 tetrahedra (*b*).

4.3.2. Thermal stability of triborate groups

The configuration of triborate groups was discussed in detail in [31]. It is almost planar, O2 and O5 oxygen atoms of BO_4 tetrahedron are situated on both sides of this plane on the distances 1.302 and 1.125 Å, both coming closer to this plane on heating (on 0.013 and 0.022 Å, heated to 227 and 377 °C, correspondingly). The O2–B2–O5 angle is stable, i.e. 109.7° at 20 and 377 °C. The B–O–B angles within triborate groups in the LiB_3O_5 structure change on heating to 377 °C by 0.2–0.9° (Table 6), the average changing of all B–O–B angles on heating being 0.9°. Hence the size and configuration of the triborate groups are essentially unchanged with temperature and these groups can be considered as rigid units like that of triborate and pentaborate groups ($[B_5O_8]^-$ double ring [23] consisting of two triborate rings linked via the tetrahedron) in α-$Na_2B_8O_{13}$ [37] and pentaborate groups in α-CsB_5O_8 [38].

4.3.3. Structural mechanism of thermal expansion

There are two non-equivalent B–O–B angles between triborate groups (Fig. 3, 4). The B1–O2–B2 angle between B–O groups within the chains B1–O2–B2 links triborate groups into screw chains along *c*-axis. This angle changes slightly (0.5°) on heating, not much more than B–O–B changing within B–O groups (0.2–0.9°). The B2–O5–B3 angle linking chains of triborate groups increases much more above 3° (Table 6). Furthermore, the shift of O5 atoms constituting this angle is more than the shifts of other oxygen atoms in the structure. As a result, the chains of triborate groups move apart leading to a high thermal expansion in *ab* plane that, in turn, leads to a simultaneous contraction along *c*-axis.

Table 6
B–O–B (°) angles in the LiB_3O_5 crystal structure at 20, 227 and 377 °C

Angles	20 °C	227 °C	377 °C	Δ*
B–O–B (°) angles within triborate groups				
B1–O1–B2	123.3(1)	123.4(2)	123.5(3)	0.2
B1–O3–B3	118.69(5)	118.4(4)	118.3(2)	−0.3
B2–O4–B3	119.81(7)	120.1(1)	120.7(2)	0.89
B–O–B (°) angles between triborate groups				
B1–O2–B2	119.1(1)	119.4(4)	119.5(6)	0.5
B2–O5–B3	124.67(8)	126.4(1)	127.8(3)	3.13
⟨B–O–B⟩	121.1	121.5	122.0	0.9

*Δ—the difference between the angles at 377 and 20 °C, accordingly.

Also we examine rotating of triborate groups as a rigid body. These groups rotate with decreasing of the dihedral angle provided by *ab* plane on 1.4° from 54.6 to 53.2° thus leading to contraction along *c*-axis. The angles with *ac* and *bc* plains increase on 0.5 and 0.9°, correspondingly. The plane of triborate group is considered to be the plane outlined through the three boron atoms. Thus, contraction along *c*-axis is likely to be realized not by changing the angles between B–O groups in the screw chains but mainly via the rotation of B–O groups' plane relative to *ab*.

The structural model of highly anisotropic thermal expansion revealed by a high-temperature X-ray diffraction is suggested. The shift of Li atoms is directed mainly along the *a*-axis causing a high thermal expansion of the structure realized by rotating of B–O rigid groups relatively to each other in the screw chains and moving of these chains apart (Figs. 3, 4). This thermal expansion is compensated by the thermal contraction along *c*-axis.

5. Conclusions

The LiB_3O_5 crystal structure was refined in the anharmonic approximation at a high temperature. A high mobility of Li atoms and their highly asymmetric vibrations are observed. The ellipsoid of Li thermal vibrations is oviform. The regular trend between the anharmonicity of Li thermal vibrations and efficiency of the second harmonic generation is observed: thermal

vibrations of Li atoms in $Li_2B_4O_7$ are more harmonic than in LiB_3O_5, for which SHG effect is more pronounced.

When a slight reduction of B–O bond lengths was corrected in a view of atomic thermal vibrations like in the case of triborate and pentaborate groups of α-$Na_2B_8O_{13}$ [37] and pentaborate groups of α-CsB_5O_8 [38] the rigid triborate groups in LiB_3O_5 donot change configuration and size on heating, but they rotate relatively to each other. Strong B–O bonds show small variations with temperature whereas the lengths of weak Li–O bonds change considerably. We describe the LiB_3O_5 structure as the framework of rigid triborate groups with flexible linkages, that helps to understand their high-temperature behavior. The LiB_3O_5 structure is viewed as a three-dimensional hinge and demonstrates the highly anisotropic thermal expansion ($\alpha_a = 101$, $\alpha_b = 31$ $\alpha_c = -71 \times 10^{-6}\,^{\circ}C^{-1}$), although the volume thermal expansion ($\alpha_v = 60 \times 10^{-6}\,^{\circ}C^{-1}$) is ordinary for borates [39].

Boron–oxygen framework expands along *ab* plane by moving apart of the chains of triborate groups realized through the change of B2–O5–B3 angle by 3.13°. The dihedral angle between triborate groups and *ab* plane decreases from 54.5 to 53.2° thus leading to the contraction along *c*-axis. The mechanism of B–O groups rotation adjusting B–O flexible framework to Li highly anisotropic thermal vibrations is disclosed. Li atoms shift to 0.26 Å on heating up to 377 °C mainly along the *a*-axis leading to a high thermal expansion in this direction.

Acknowledgments

This research has been supported by the Russian Foundation for Basic Research, No. 05-03-33246.

References

[1] S. Lin, Z. Sun, B. Wu, C. Chen, J. Appl. Phys. 67 (1990) 634.
[2] T. Ukachi, R.J. Lane, W.R. Bosenberg, C.L. Tang, Appl. Phys. Lett. 57 (10) (1990) 980–982.
[3] S.P. Velsko, M. Webb, C. Huang, IEEE J. Quantum Electron. 27 (9) (1991) 2182–2192.
[4] I.N. Ogorodnikov, L.I. Isaenko, A.V. Kruzhalov, A.V. Porotnikov, Radiat. Meas. 33 (2001) 577–581.
[5] I.N. Ogorodnikov, V.Yu. Yakovlev, L.I. Isaenko, Phys. Solid State 45 (5) (2003) 845–853.
[6] S. Matyiasik, Yu.V. Shaldin, Solid State Phys. 43 (8) (2001) 1405–1408 (in Russian).
[7] Y. Wang, Y.J. Jiang, Y.L. Liu, L.Z. Zeng, Appl. Phys. Lett. 67 (17) (1995) 2462–2464.
[8] Y. Furukawa, S.A. Markgraf, M. Sato, H. Yoshida, T. Sasaki, H. Fujita, T. Yamanaka, S. Nakai, Appl. Phys. Lett. 65 (12) (1994) 1480–1482.
[9] E. Betourne, M. Touboul, J. Alloys Comp. 255 (1997) 91–97.
[10] S.C. Sabharwal, B. Tiwari, Sangeeta, J. Crystal Growth 249 (2003) 502–506.
[11] N. Pylneva, V. Kosyakov, A. Yurkin, G. Bazarova, V. Atuchin, A. Kolesnikov, E. Trukhanov, C. Zilling, Crys. Res. Technol. 36 (12) (2001) 1377–1384.
[12] H.G. Kim, J.K. Kang, S.J. Chung, The XVII Congress and General Assembly of the International Union of Crystallography, Washington, USA, August 8–17, 1996.
[13] U. Moryc, W.S. Ptak, J. Molec. Structure 511–512 (1999) 241–249.
[14] H.R. Xia, L.X. Li, H. Yu, S.M. Dong, J.Y. Wang, Q.M. Lu, C.Q. Ma, X.N. Wang, J. Mater. Res. 16 (12) (2001) 3464–3470.
[15] Ji Won Kim, Choon Sup Yoon, H.G. Gallagher, Appl. Phys. Lett. 71 (22) (1997) 3212–3214.
[16] A.U. Sheleg, T.I. Dekola, N.P. Tekhanovich, A.M. Luginets, Phys. Solid State 39 (4) (1997) 545–546.
[17] V.V. Atuchin, L.D. Pokrovsky, V.G. Kesler, L.I. Isaenko, L.I. Gubenko, J. Ceram. Process. Res. 4 (2) (2003) 84–87.
[18] M. Ihara, M. Yuge, J. Krogh-Moe, J. Ceram. Soc. Jpn. 88 (1980) 179.
[19] H. Koenig, R. Hoppe, Z. Anorg. Allge. Chem. 439 (1978) 71–79.
[20] S.F. Radaev, E.A. Genkina, V.A. Lomonov, B.A. Maksimov, Yu.V. Pisarevskii, M.N. Chelnokov, V.I. Simonov, Kristallografiya 36 (1991) 1419–1426.
[21] S.F. Radaev, B.A. Maximov, V.I. Simonov, B.V. Andreev, V.A. D'yakov, Acta Crystallogr. B 48 (1992) 154–160.
[22] C. le Henaff, N.K. Hansen, J. Protas, G. Marnier, Acta Crystallogra. B 53 (1997) 870–879.
[23] J. Krogh-Moe, Phys. Chem. Glasses 6 (1965) 46–54.
[24] J. Krogh-Moe, Acta Crystallogra. B 30 (1974) 747.
[25] J. Krogh-Moe, Acta Crystallogra. B 28 (1972) 1571.
[26] J. Krogh-Moe, Acta Crystallogra. B 13 (1960) 889–892.
[27] J. Krogh-Moe, Acta Crystallogra. B 30 (1974) 1178–1180.
[28] T. Sasaki, Y. Mori, I. Kuroda, S. Nakajima, K. Yamaguchi, S. Watanabe, S. Nakai, Acta Crystallogr. C (39,1983-) (1995) 51, 2222–2224.
[29] M. Touboul, E. Betourne, G. Novogorocki, J. Solid State Chem. 131 (1997) 370–373.
[30] R.S. Bubnova, I.G. Polyakova, M.G. Krzhizhanovskaya, V.B. Trofimov, S.K. Filatov, Inorganic Mater. 34 (1998) 1328–1334 (in Russian).
[31] M.G. Krzhizhanovskaya, R.S. Bubnova, V.S. Fundamensky, I.I. Bannova, I.G. Polyakova, S.K. Filatov, Crystallogr. Rep. 43 (1) (1998) 21–25.
[32] R.S. Bubnova, V.S. Fundamensky, I.I. Bannova, I.G. Polyakova, Yu.G. Shturmer, S.K. Filatov, Dokl. Phys. Chem. 398 (2) (2004) 249–253.
[33] D. Xue, K. Betzler, H. Hesse, Appl. Phys. A 74 (6) (2002) 779–782.
[34] Z. Lee, J. Lin, Z. Wang, Ch. Chen, M.H. Lee, Phys. Rev. B 62 (3) (1999) 1757–1764.
[35] Lin Wei, Dai Guiquing, Huang Qingzhen, Zhen An, Liang Jingkui, J. Phys. D 23 (1990) 1073.
[36] M.D. Mathews, A.K. Tyagi, P.N. Moorthy, Thermochim. Acta 319 (1998) 113–121;
M.D. Mathews, A.K. Tyagi, P.N. Moorthy, Thermochim. Acta 320 (1998) 89–95.
[37] R.S. Bubnova, Yu.F. Shepelev, N.A. Sennova, S.K. Filatov, Z. Krist. Crys. 217 (2002) 444.
[38] S. Filatov, R. Bubnova, Yu. Shepelev, J. Anderson, Yu. Smolin, Crystal Res. Technol. 40 (2005) 65.
[39] S.K. Filatov, R.S. Bubnova, Phys. Chem. Glasses 41 (2000) 216.
[40] J.A. Ibers, W.C. Hamilton, (Eds.) International Tables for X-ray crystallography, vol. IV, International Union of Crystallography, vol. 365, 1974, p. 7.
[41] W.R. Busing, K.O. Martin, H.A. Levy, Osk Ridge National Laboratory Report ornl-TM-306, Tenesse, 1962.
[42] V.I. Andrianov, Kristallografiya 32 (1) (1987) 228.
[43] V.G. Zirelson, Crystal Chem. 27 (1) (1993) 268 (in Russian).
[44] B.S. Sastry, E.A. Hummel, J. Amer. Ceram. Soc. 41 (1) (1958) 7.

[45] A.B. Kaplun, A.B. Meshalkin, J. Crystal Growth 209 (2000) 890–894.
[46] J. Aidong, L. Shirong, H. Qingzhen, C. Tianbin, K. Deming, Acta Crystallogr. C 46 (1990) 1999.
[47] A.P. Rollet, R. Bouaziz, Compt. Rend. Acad. Sci. 240 (25) (1955) 2417–2419.
[48] O.V. Masurin, M.V. Strelnitskaya, T.P. Shvaiko-Shvaikovskaya, Reference Book 5 (1987) 226 (in Russian).
[49] R.S. Bubnova, I.G. Polyakova, Yu.E. Anderson, S.K. Filatov, Phys. Chem. Glasses 25 (1999) 2 (in Russian).
[50] D.Yu. Pushcharovsky, E.R. Gobetchia, M. Pasero, S. Merlino, O.V. Dimitrova, J. Alloys Compods. 339 (2002) 70.
[51] N.A. Sennova, R.S. Bubnova, Ju.F. Shepelev, S.K. Filatov, O.I. Yakovleva, private communications.
[52] M. Cameron, S. Sueno, C.T. Prewitt, J.J. Papike, Am. Mineral. 58 (1973) 594.
[53] N.E. Brese, M. O'Keeffe, Acta Crystallogr. B 47 (1991) 192.
[54] S.A.T. Redfern, in: R.M. Hazen, R.T. Downs (Eds.), High-Temperature and High-Pressure Crystal Chemistry, Reviews in Mineralogy, vol. 41. Mineralogical Society of America, Washington, 2000, pp. 289–308.
[55] D.L. Corker, A.M. Glazer, Acta Crystallogr. B 25 (1996) 260–265.
[56] P.S. Burns, J.D. Grice, F.C. Hawthorne, Can. Miner. 22 (1995) 1131.
[57] J.A. Ibers, W.C. Hamilton (Eds.), International Tables for X-ray Crystallography, vol. IV, International Union of Crystallography, 1974, p. 365.
[58] R.T. Downs, G.V. Gibbs, K.L. Bartelmehs, M.B. Boisen, Am. Mineral. 77 (1992) 751–757.
[59] R.T. Downs, in: R.M. Hazen, R.T. Downs (Eds.), High-Temperature and High-Pressure Crystal Chemistry, Reviews in Mineralogy, vol. 41. Mineralogical Society of America, Washington, 2000, pp. 61–87.